Deflection of O_2^+ ion flow by the Martian Magnetic Fields

Shibang Li[1], Haoyu Lu[1,2†], Jinbin Cao[1,2], Jun Cui[3], Chenling Zhou[1], James A. Wild[4], Guokan Li[1], Yun Li[1,2]

[1]School of Space and Environment, Beihang University, Beijing, 100191, China

[2]Key Laboratory of Space Environment Monitoring and Information Processing, Ministry of Industry and Information Technology, Beijing, 100191, China

[3]School of Atmospheric Sciences, Sun Yat-Sen University, Zhuhai, China

[4]Department of Physics, Lancaster University, Lancaster, UK

†Correspondence to H. Y. Lu at lvhy@buaa.edu.cn

Abstract.

The effect of the Martian crustal magnetic field on ion escape is the focus of considerable interest. Directions of Martian magnetic field determined by the interaction between Mars' crustal and interplanetary magnetic fields have been suggested to play a significant role on ion transport around Mars. In this study we investigate the physical mechanism deflecting O_2^+ transport in two typical magnetic field orientations at horizontal plane by performing three-dimensional multi-fluid Hall magneto-hydrodynamic (MHD) simulations. Cross validation of the simulation results from G110 crustal field model and equivalent source dipole model reveals that due to the Hall electric force, O_2^+ ions flow tends to be accelerated eastwards in the region occupied by outward magnetic fields, and westwards in the region with inward magnetic fields. These results are helpful for understanding how the deflection of Martian atmospheric ions flow are influenced by the Martian magnetic field environment and the impact of the crustal fields on the motion of atmospheric ions in the Martian space environment.

Keywords

Mars, Solar-planetary interactions, Magnetic anomalies, Magnetohydrodynamics

1. Introduction

The mechanisms that have caused the Martian atmosphere to evolve from Earth-like to the present situation have been a topic of considerable debate since the first probes arrived at the planet. Compared to the Earth, Mars is further away from the Sun and does not possess an intrinsic magnetic field. Although the substantial intrinsic magnetic field on Earth can block high-energy particles in solar wind and prevent planetary ions from escaping, the terrestrial magnetic field is not necessarily needed to protect the planetary atmosphere from erosion by the solar wind (Ramstad et al., 2021). Indeed, the presence of the intrinsic magnetic field appears to increase the ion escape rate for most levels of magnetization and solar wind conditions (Gunell et al., 2018; Ramstad et al., 2021). Furthermore, the relationship between the strength of the intrinsic magnetic field and the magnetic standoff distance indicates that the relative position between the standoff distance and the induced magnetosphere determines the enhancing/inhibiting effect of the intrinsic magnetic field on the ion escape rate (Egan et al., 2019; Sakata et al., 2020).

Despite the fact that Mars lacks a global intrinsic magnetic field, it possesses local magnetic fields on its surface, primarily distributed in the southern hemisphere with the strongest located at east longitude around 180° (Acuña et al., 1999). The presence and asymmetric distribution of these crustal fields introduce great complexity into the plasma dynamics of the Martian environment, resulting in a disordered magnetic field topology (Xu et al., 2016; Weber et al., 2020). Observational analysis reveals three magnetic field topologies in the Martian plasma environment, i.e., closed, open and draped (Brain et al., 2007; Duru et al., 2011; Weber et al., 2020; Xu et al., 2017). Xu et al. (2019) have suggested that below an altitude of 1200 km, the dominant magnetic topology over strong crustal fields on the dayside is the so-called closed-to-day, with vertical magnetic field lines at two ends embedded in the collisional atmosphere, between which horizontal magnetic field lines exist. Previous studies have also shown that the direction of the magnetic field has a significant impact on the ion transport. The diffusion of ionospheric plasma tends to be suppressed around the region dominated with horizontal magnetic field lines, confirmed by 2D ionospheric simulations (Matta et al., 2015). On the other hand, vertical magnetic field lines tend to promote plasma to high altitudes.

Based on observational analysis from the Mars Express (MEX) mission, hyperbola-shaped traces in the echogram and dual traces in the ionogram have been repeatedly observed above regions with vertical and strong crustal magnetic fields (e.g., Duru et al., 2006; Gurnett et al., 2005; Andrews et al., 2014; Diéval et al., 2018), interpreted as indications of ionospheric upwelling. This has been demonstrated to be a result of field-aligned plasma diffusion and characterized by an increase in electron density (Matta et al., 2015). Meanwhile, by statistically analyzing data from Mars Atmosphere and Volatile EvolutioN (MAVEN) mission, Wu et al (2019) have confirmed that vertical magnetic field lines tend to cluster around strong magnetic anomalies on Mars and the ion distributions for near-vertical field lines are more extended than those for near-horizontal field lines. Moreover, the global-scale ion transport around Mars can also be affected by the crustal field in the horizontal plane, causing deflection of the ion flows in the southern hemisphere (Fan et al., 2020).

While the previously reported results show that there exists a strong dependence between the magnetic field direction and ion transport, the physical mechanism behind this phenomenon is not fully understood, especially the deflection effect due to Martian crustal field in the horizontal plane. While there have been many models in order to study the interaction between solar wind and Mars (e.g., Ma et al., 2004; Najib et al., 2011; Dong et al., 2014; Li Y. et al., 2021) and the impact of crustal magnetic fields on modifying global Martian ion escape rate (e.g., Fang et al., 2015, 2017), few self-consistent global simulations of Mars-solar wind interaction devote to resolve the physical mechanism of the impact of magnetic field orientations on the ion transport deflection. In this study, by investigating the ion dynamics and electromagnetic forces in the regions occupied by the Martian crustal magnetic field, we show how two typical orientations of the magnetic field affect plasma transport around Mars. Our results contribute to the understanding of how the deflecting direction of Martian atmospheric ions flow is influenced by the orientation of magnetic field.

2. Model Description

The 3-D multi-fluid MHD Model used in this study solves separate mass, momentum and energy equations for the four main ion species in the Martian ionosphere, i.e., H^+, O_2^+, O^+, CO_2^+. The governing equations for ion species *s* can be expressed as follows (Najib et al., 2011, Li et al., 2022):

$$\frac{\partial \rho_s}{\partial t} + \nabla \cdot (\rho_s \boldsymbol{u_s}) = \frac{\delta \rho_s}{\delta t} \tag{1a}$$

$$\frac{\partial(\rho_s \boldsymbol{u_s})}{\partial t} + \nabla \cdot (\rho_s \boldsymbol{u_s} \boldsymbol{u_s} + \boldsymbol{I} p_s) = n_s q_s (\boldsymbol{u_s} - \boldsymbol{u_+}) \times \boldsymbol{B} + \frac{n_s q_s}{n_e e}(\boldsymbol{J} \times \boldsymbol{B} - \boldsymbol{\nabla} p_e) + \frac{\delta M_s}{\delta t} \tag{1b}$$

$$\frac{\partial e_s}{\partial t} + \nabla \cdot [(e_s + p_s)\boldsymbol{u_s}] = \boldsymbol{u_s} \cdot \left[n_s q_s (\boldsymbol{u_s} - \boldsymbol{u_+}) \times \boldsymbol{B} + \frac{n_s q_s}{n_e e}(\boldsymbol{J} \times \boldsymbol{B} - \boldsymbol{\nabla} p_e)\right] + \frac{\delta E_s}{\delta t} \tag{1c}$$

where $\mathrm{e}_s = \frac{1}{2}\rho_s \boldsymbol{u}_s^2 + \frac{p_s}{\gamma - 1}$. Here $\rho_s, \boldsymbol{u_s}, p_s, n_s$ and q_s are the individual mass density, velocity, pressure of the ions, number density and charge respectively. $\boldsymbol{B}$ is the magnetic field, $\boldsymbol{I}$ is the identity matrix, γ is the polytropic index chosen to be 5/3. $p_e = \sum_{i=ions} p_i$, $n_e = \sum_{i=ions} n_i$ are the pressure and number density of electrons. The electric current density can be obtained from $\boldsymbol{J} = \frac{1}{\mu_0} \nabla \times \boldsymbol{B}$.

The source terms $\frac{\delta \rho_s}{\delta t}$, $\frac{\delta M_s}{\delta t}$ and $\frac{\delta E_s}{\delta t}$ on the right side of Equation (1), respectively represent the variations of mass, momentum and energy due to the collisions and chemical reactions among all the species (Li et al., 2020), where the inelastic collisions include three chemical reactions of charge exchange, photoionization and recombination, with the corresponding reaction rates adopted from Ma et al., (2004) and Schunk and Nagy (2009). The photoionization effect was included by adopting the Chapman function method, which has been proved to significantly improve the agreement with the plasma density observations (Ma et al., 2015).

By introducing the charge-averaged ion velocity $\boldsymbol{u_+} = \frac{1}{e n_e} \sum_s n_s q_s \boldsymbol{u_s}$ and electron velocity $\boldsymbol{u_e} = \boldsymbol{u_+} - \frac{\boldsymbol{J}}{e n_e}$, the magnetic induction equation can be written as:

$$\frac{\partial \boldsymbol{B}}{\partial t} - \nabla \times \left(\boldsymbol{u_+} \times \boldsymbol{B} - \frac{\boldsymbol{J} \times \boldsymbol{B}}{e n_e} + \frac{\boldsymbol{\nabla} p_e}{e n_e}\right) = 0 \tag{2}$$

It should be noted that the electromagnetic (EM) forces acting on the O_2^+ ion can be derived from the plasma momentum equations of Equation (1b), which has the form as follows:

$$\boldsymbol{F}_{\boldsymbol{EMO}_2^+} = n_s q_s(\boldsymbol{u_s} - \boldsymbol{u}_+) \times \boldsymbol{B} + \frac{n_s q_s}{n_e e}\boldsymbol{J} \times \boldsymbol{B} - \frac{n_s q_s}{n_e e}\boldsymbol{\nabla} p_e \quad (3)$$

The three terms on the right side of Equation (3) respectively correspond to motional electric force, Hall electric force and ambipolar electric force. It is noteworthy that the magnetic field is moving with average ion velocity (u_+), so the motional electric force on O_2^+ depends on its relative velocity to u_+ (Ma et al., 2019).

The Mars-centered Solar Orbital (MSO) reference frame was adopted in our simulations, where the *x* axis points from Mars towards the Sun($-24R_M \leq X_{MSO} \leq 8R_M$), the *z* axis is perpendicular to the *x* axis and positive toward the north celestial pole, the *y* axis completes the right-handed coordinate system($-16R_M \leq Y_{MSO}, Z_{MSO} \leq 16R_M$). The total number of computational cells is 960,000 with the finest cell of 10 km at the lowest inner boundary. In case of analyzing the ion dynamics in the horizontal plane at a certain altitude, the spherical coordinates (r, θ, φ) transformed from the MSO was adopted where *r* points radially outward, θ points southward, and φ points eastward. According to the typical solar wind parameters in upstream of Mars (Dong et al., 2014; Liu et al., 2021), the solar wind density and velocity were chosen to be $4\ cm^{-3}$ and 500 km/s, respectively. The IMF was assumed to be a Parker spiral orientation of 56° with magnitude of 3 nT in the *x-y* plane, i.e., $(B_x, B_y, B_z) = (-1.6, 2.5, 0)\ nT$ in the MSO coordinate system. We adopted the 110° harmonic expansion for the crustal magnetic field developed by Gao et al., (2021) to describe the observed fields at Mars (Acuña et al., 1999). The subsolar point is 180° longitude at the equator, corresponding to $(X_{MSO}, Y_{MSO}, Z_{MSO}) = (X, 0, 0)R_M$, where $1 \leq X \leq 8$.

Moreover, equivalent source dipole (ESD) is one of general methods for building the crustal magnetic field on Mars (Li X. Z. et al., 2020), and fits the observed magnetic field with an equivalent strength distribution of magnetic dipoles. The structure of the magnetic dipole is nearly the same as the closed-to-day topology that has two vertical-line regions at two ends embedded in Martian ionosphere, between which is the horizontal-line region in the center. Therefore, in order to verify the physical mechanism and impact of magnetic field orientations on O_2^+ deflecting direction, we placed an ESD below the surface of 180° longitude and -53° latitude with the equivalent strength of the real strongest Martian anomaly to mimic closed-to-day magnetic field topology. Expressions of the magnetic field for the ESD are as follows:

$$B_x = 3(x - x_0)(y - y_0)M_y r^{-5}, \quad (4a)$$

$$B_y = (3(y - y_0)^2 - r^2)M_y r^{-5}, \quad (4b)$$

$$B_z = 3(z - z_0)(y - y_0)M_y r^{-5}, \quad (4c)$$

where M_y and *r*, respectively, denote the magnetic moment along the *y* axis and the altitude above the Martian surface. The point (x_0, y_0, z_0) in the MSO coordinate represents the center of the dipole field. The $M_y = 6 \times 10^{10} nT \cdot km^3$ and $(x_0, y_0, z_0) = (1840\ km, 0, -2441\ km)$ were chosen, which means that the ESD is located at $53^{\circ} S$ with roughly 180 nT magnitude at 350 km altitude, which is approximately consistent with the observational value of the actual crustal magnetic field. Figures in Appendix A provide the magnetic field topology of the ESD around Mars and the distributions of the total magnetic field strength and inclination angle at 350 km, resulting from observations and simulations with the crustal magnetic field representation of ESD and the Gao et al. (2021) model, respectively.

3. Simulation Results

The O_2^+ ion is one of the dominant species in the Martian ionosphere (Withers et al., 2019; Inui et al., 2019; Sakai et al., 2018) and ion transport is a critical factor in the ion escape mechanism at Mars. On the one hand, at high altitude (above 200 km) ion transport dominates (Mendillo et al. 2011; Chaufray et al. 2014) and the ion flow tends to be deflected by the crustal field in the horizontal plane (Fan et al., 2020). On the other hand, the ion distribution can be affected by the diffusion process associated with the orientation of magnetic field (Wu et al., 2019; Matta et al., 2015). In order to demonstrate the deflection impact of Martian crustal magnetic field on the O_2^+ ion flow, we transformed our numerical result from MSO coordinates into the spherical coordinates and extracted dayside horizontal velocity vector (black) of O_2^+ ions mapped on the distribution of Martian crustal field isomagnetic lines (grey) at 350 km, as shown in Figure 1, which was obtained from numerical run with G110 model. It is obvious that the ion flow in the southern hemisphere is deflected to the eastward/westward by the crustal magnetic fields and the magnitude is smaller than in the northern hemisphere, which are consistent with previous observations (Fan et al., 2020). Since the distribution of O_2^+ velocity in the northern and southern hemisphere are supposed to be equatorially symmetric in absence of crustal field (shown in Appendix B), it is the Martian crustal fields that deflect the direction of O_2^+ ions flow in the southern hemisphere. Moreover, the eastward and westward ions flows appear alternately around the strongest crustal field region marked by a dashed orange rectangle. This feature is similar to the orientation of Martian magnetic fields as shown in Appendix Figures A3(a) and A3(b), both the observations and simulation confirm that the inward and outward magnetic fields are also dominant alternatively in the same area. Therefore, it is reasonable to believe that there is a correlation between the deflection direction of the O_2^+ ions flow and the orientation of the magnetic field.

The magnetic inclination angle, defined as the angle that the local total magnetic field vector makes with the horizontal plane, was used to study the relevance of the deflection direction of ions flow to their surrounding magnetic field environment. Large absolute value of magnetic inclination angle presents vertical magnetic field whereas smaller one denotes near-horizontal field, additionally positive value of magnetic inclination angle indicates outward magnetic field whereas negative values means inward magnetic field. Figures 2a, 2b and 2c respectively show the variations of the eastward O_2^+ velocity (U_φ), the magnetic inclination angle and eastward EM Forces (F_φ) exerted on O_2^+ ions at 350 km with latitude from -90° to 0°, extracted at longitude of 180°. The grey highlights in Figure 2 represents the strong crustal field region, corresponding to the center line of dashed orange rectangle in Figure 1. From Figure 2(a) it can be seen that the U_φ changes from positive to negative, then to positive with increasing latitude in the strong crustal field region, which shows a similar variation tendency of magnetic field inclination angle as revealed by Figure 2(b). Additionally, in order to analyze the EM forces acting on the ions in detail, the eastward components of the total forces expressed as in Equation (3) were plotted in Figure 2c, which shows that the total F_φ is mainly provided by the Hall electric force. Moreover, comparison between Figures 2(b) and 2(c) shows that the magnetic inclination angle almost has the same sign as the total F_{φ}, especially in the strong crustal field region. The similar variation tendency between U_{φ}, F_{φ} and magnetic inclination angle in the strong crustal field region implies that the ion flow tends to be accelerated by the eastward EM forces in the regions with outward magnetic field, while in the regions with inward magnetic field, ion flow can be accelerated by the westward EM forces.

In order to figure out the correspondence between the orientation of magnetic field and the direction of total EM F_{φ} exerted on O_2^+ ions. Here, we respectively defined regions with outward and inward magnetic fields as with inclination angle higher than 10° and smaller than -10°. Figure 3 demonstrates the dayside southern hemisphere distribution of positive (Fig.3a) and negative (Fig. 3b) total EM F_{φ} in latitude from 0° to -90° and longitude from 90° to 270° at altitude of 350 km, superimposed by red and blue dashed contour lines with 10° and -10° magnetic inclination angle respectively. Comparison of F_{φ} distribution for the two different types of magnetic field regions in Figure 3 indicates that the positive F_{φ} dominates in the region with outward magnetic field, which can speed up ions flow eastwards, while in the region with inward magnetic field, the negative F_{φ} is dominant and can speed up ions flow westwards .

Due to the irregularity and narrow, strip-like distribution of the Martian crustal field, the regions occupied by magnetic field with different orientations are difficult to distinguish (as shown in Appendix Figures A3(a) and A3(b)), which motivated us to adopt a simplified dipole model to cross-validate the roles and mechanisms of orientation of magnetic field in deflecting the ion transport. Since the magnetic moment we adopted is along the y axis, there is an apparent outward (inward) magnetic field region in the Martian western (eastern) hemisphere and these two regions have the same magnetic field strength, which facilitates the clarification of the impact and mechanism of orientations of magnetic field on the ion flow deflection.

Figure 4 shows the dayside O_2^+ velocity vector mapped on the distribution of magnetic inclination angle in the horizontal plane at 350 km for the case with ESD model. It can be seen that the pattern of O_2^+ ions flow in the northern hemisphere is similar to that in the case without crustal field model (shown in Appendix B). The magnitude of O_2^+ velocity in the southern hemisphere is smaller than the counterpart of the northern one, especially in the vicinity of the central position of ESD. Meanwhile, O_2^+ flow deflects to eastward in the outward magnetic field region,marked with red rectangle in Fig. 4, and westward in the inward magnetic field region with blue. Thus, the deflection direction of O_2^+ ions flow in the horizontal plane depends on the orientation of magnetic fields.

Figure 5a demonstrates the distribution of magnetic inclination angle in latitude from -30° to -60° and longitude from 160° to 200° at altitude of 350 km for the cases with ESD model. Figures 5b, 5c and 5d respectively show the variations of the magnetic inclination angle, the eastward O_2^+ velocity (U_{φ}) and eastward EM Forces (F_{φ}) exerted on O_2^+ ions with longitude, extracted at latitude of -50° from Figure 5a (white line). We respectively defined outward and inward magnetic field regions as with elevation angles higher and smaller than 0°, which are highlighted in Figures 5b to 5d in orange and blue. U_{φ} and F_{φ} have opposite signs on either side, and are approximately zero in the central position of ESD. In the outward field region with longitude of 160° to 180°, both U_{φ} and F_{φ} are in the eastward direction, indicating that O_2^+ ions are being accelerated eastwards in this region. In addition, both U_{φ} and F_{φ} are in the westward direction in the inward field region with longitude of 180° to 200°, indicating that O_2^+ ions are being accelerated westwards there. It can be seen from Figure 5d that the dominant force in the φ direction is Hall electric force. Therefore, the simulation results obtained by considering the ESD model reinforce the conclusions derived from the case with G110 model.

4. Discussion and Conclusion

The well-developed MHD model employed in this study is able to self-consistently reproduce the Martian ionosphere by including the production and loss processes of the main ionospheric ion species through considering physical collisions and chemical reactions among these species. In order to investigate the impact of orientations of magnetic field on O_2^+ ions flow deflection, Gao's crustal field model (G110) and an equivalent source dipole (ESD) model with similar strength and position of the strongest crustal field were adopted to cross-validate physical mechanisms behind the phenomena with each other.

Results from numerical simulations indicate that there exists a strong correspondence between the direction of O_2^+ ions transport and the orientation of magnetic field. Magnetic fields can deflect the flow of O_2^+ ions, i.e., O_2^+ ions flow tends to be accelerated towards the east in the outward magnetic field region and west in the inward one. The controlling force is mainly contributed by the Hall electric force, which provides an explanation for the deflection effect of the Martian crustal fields observed by MAVEN (Fan et al., 2020).

Although our simulation results revealed that the Hall electric field has a significant impact on deflecting ions flow in the outward/inward magnetic field region, the distributions of O_2^+ velocity in the northern and southern hemisphere at a certain altitude are equatorially symmetric in absence of crustal field as shown in Appendix B, meaning that there is no deflection effect in the horizontal magnetic field region formed by draping interplanetary magnetic field. In other words, only outward/inward magnetic field formed by the interaction of interplanetary magnetic field and the Martian crustal field deflects ions motion in the horizontal plane. Moreover, the orientation of the interplanetary magnetic field and the rotation of the crustal field with Mars have a significant impact on the Martian magnetic field environment, which in turn affects the ion motion and deserves further investigation.

Acknowledgement.

The magnetic field (MAG) were obtained from the MAVEN "key parameter" summary data available from the CDAWeb database at https://cdaweb.gsfc.nasa.gov/index.html/. This work was supported by the B-type Strategic Priority Program of the Chinese Academy of Sciences (Grant No. XDB41000000) and the pre-research projects on Civil Aerospace Technologies No. D020103 and D020105 funded by China's National Space Administration (CNSA), and the National Natural

Science Foundation of China (NSFC) under grant No. 42074214. JAW was supported by STFC Consolidated Grant ST/R000816/1.

Figure captions

Figure 1. Dayside O_2^+ ion velocity vector (black anchor) overlapped on isomagnetic lines (grey) of the Martian crustal field in the horizontal plane at 350 km, resulting from simulation with Gao's crustal field model.

Figure 2. Distributions of variables resulting from simulation with Gao's crustal field model at 350 km. The variation of (a) eastward velocity (U_φ), (b) magnetic field inclination angle, (c) eastward total electro-magnetic forces (F_φ, red line) and Hall electric force (green line) along latitude at longitude of 180°.

Figure 3. Dayside southern hemisphere distribution of positive (a) and negative (b) total EM F_φ in latitude from 0° to -90° and longitude from 90° to 270° at altitude of 350 km accompanied by red and blue dashed contour lines of 10° and -10° magnetic inclination angle separately, resulting from simulation with Gao's crustal field model.

Figure 4. Magnetic elevation angle in the longitude-latitude plane at 350 km from results of simulations with ESD model. Black anchor represents the dayside velocity vector of O_2^+.

Figure 5. Distributions of variables resulting from simulation with ESD model at 350 km. (a) magnetic elevation angle in latitude from -30° to -60° and longitude from 160° to 200°. (b) magnetic elevation angle, (c) eastward velocity, (d) eastward EM forces, along the white line of Figure 5a at latitude of -50°. Orange and blue highlights represent the outward and inward magnetic field regions respectively.

Figure 1

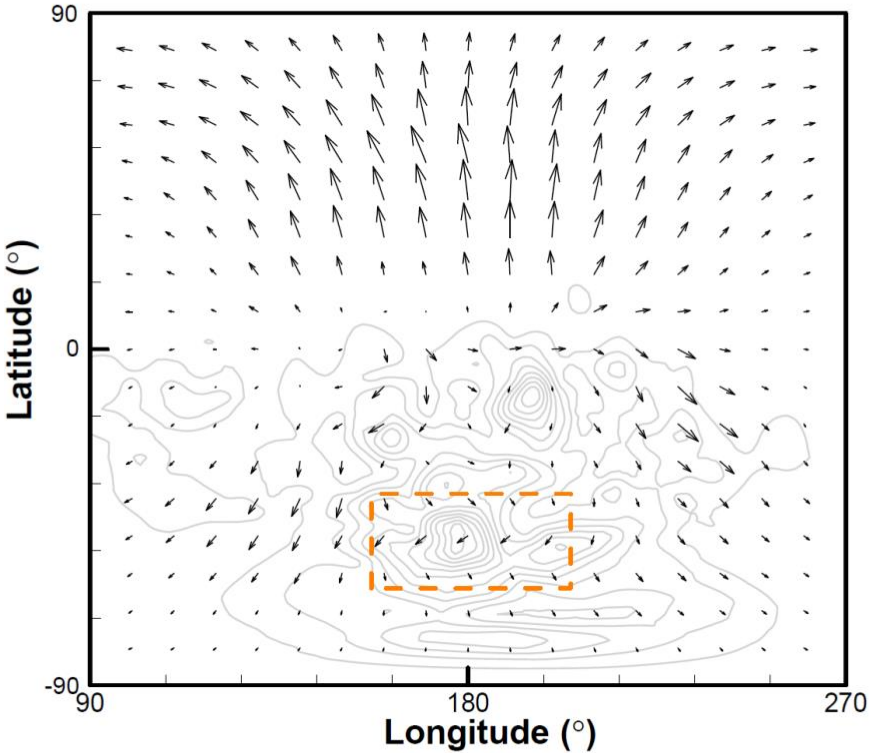

Figure 2

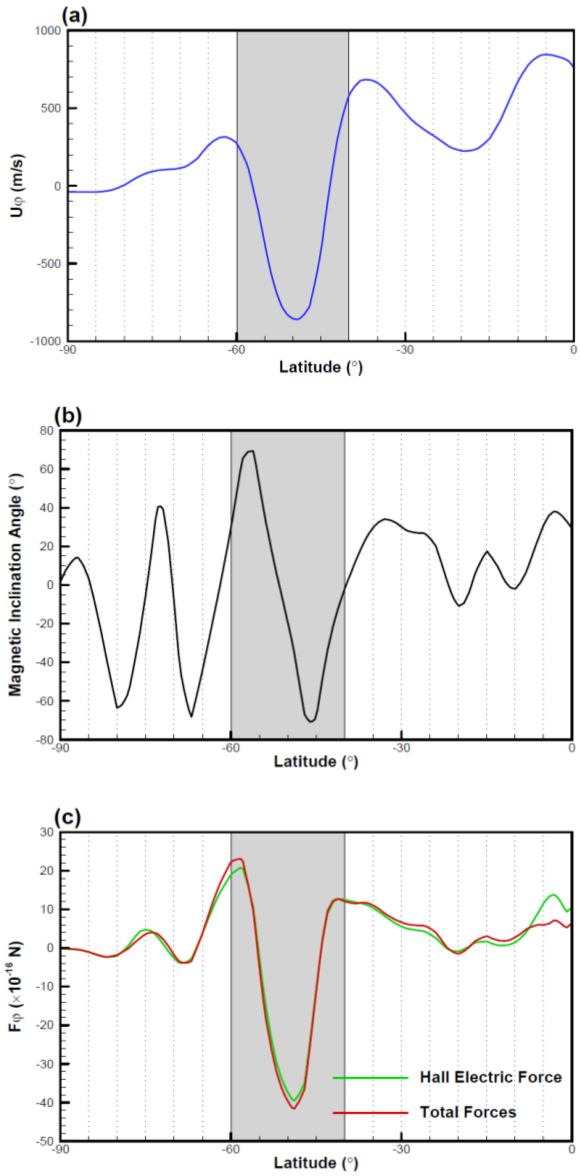
(a)
Uφ (m/s)
1000
500
0
-500
-1000
-90
-60
-30
0
Latitude (°)
(b)
Magnetic Inclination Angle (°)
80
60
40
20
0
-20
-40
-60
-80
-90
-60
-30
0
Latitude (°)
(c)
Fφ (×10^-16 N)
30
20
10
0
-10
-20
-30
-40
-50
-90
-60
-30
0
Latitude (°)
Hall Electric Force
Total Forces

Figure 3

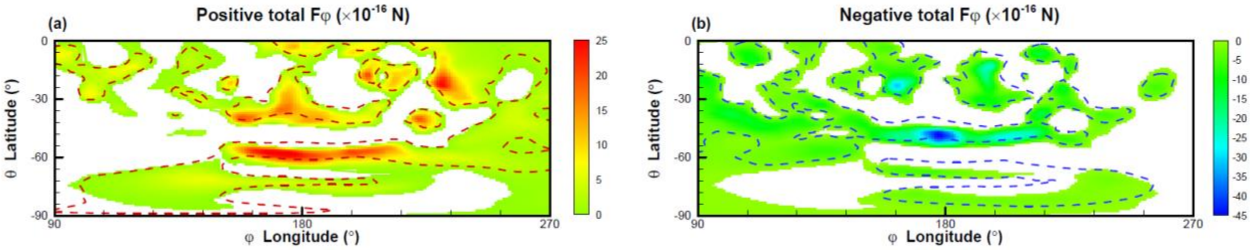

(a)
Positive total Fφ (×10^-16 N)
θ Latitude (°)
φ Longitude (°)
0
-30
-60
-90
90
180
270
25
20
15
10
5
0
(b)
Negative total Fφ (×10^-16 N)
θ Latitude (°)
φ Longitude (°)
0
-5
-10
-15
-20
-25
-30
-35
-40
-45

Figure 4

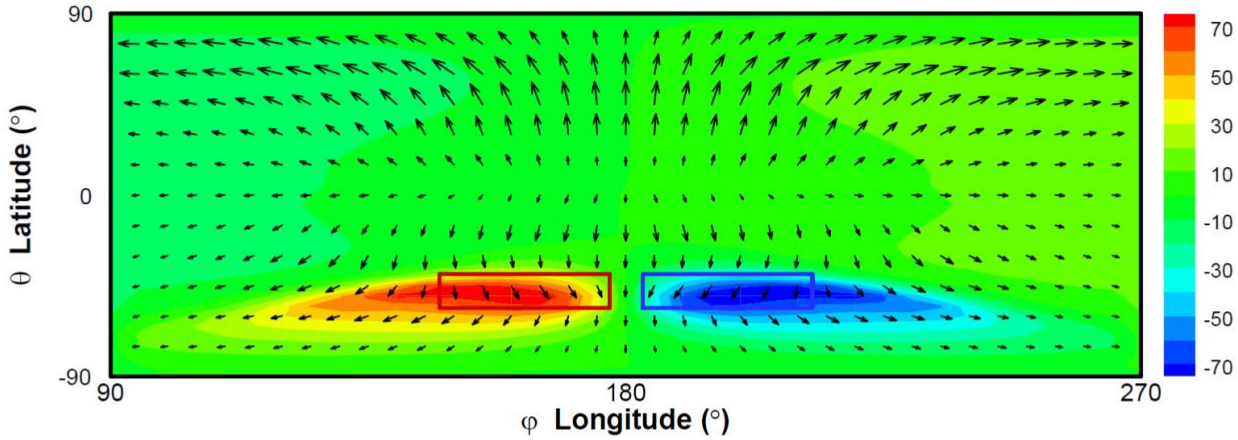

Figure 5

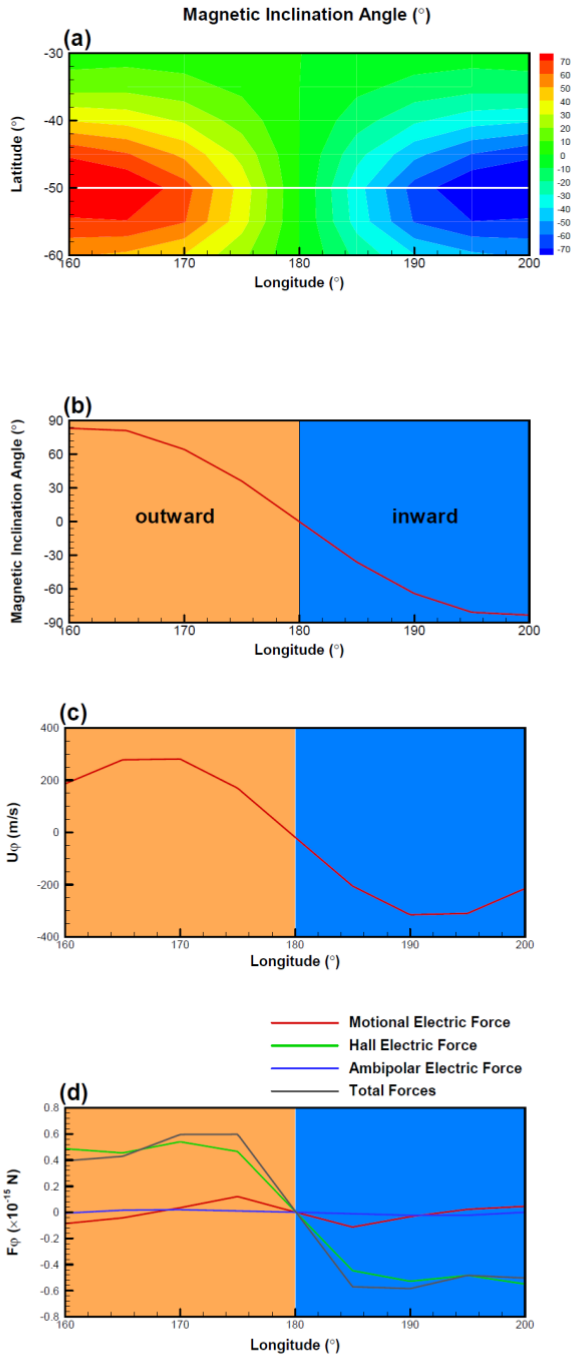

Magnetic Inclination Angle (°)
(a)
Latitude (°)
Longitude (°)
(b)
Magnetic Inclination Angle (°)
outward
inward
Longitude (°)
(c)
Uφ (m/s)
Longitude (°)
Motional Electric Force
Hall Electric Force
Ambipolar Electric Force
Total Forces
(d)
Fφ (×10⁻¹⁵ N)
Longitude (°)

References

Acuña, M. H., Connerney, J. E. P., Ness, N. F., et al. 1999, Science, 284(5415), 790–793.

Andersson, L., Ergun, R. E., Delory, G. T., et al. 2015, Space Science Reviews, 195, 173–198

Andrews, D. J., Opgenoorth, H. J., Edberg, N. J. T., et al. 2013, JGR, 118, 6228–6242.

Andrews, D. J., André, M., Opgenoorth, H. J., et al. 2014, JGR, 119, 3944–3960.

Brain, D., Lillis, R., Mitchell, D., et al. 2007, JGR, 112, A09201.

Cain, J. C., Ferguson, B. B., & Mozzoni, D. 2003, JGRE, 108, 5008

Chaufray, J.-Y., Gonzalez-Galindo, F., Forget, F., et al. 2014, JGR, 119, 1614– 1636.

Davis, J. M., Balme, M., Grindrod, P. M., et al. 2016, Geology, 44(10), 847–850.

Diéval, C., Kopf, A. J., & Wild, J. A. 2018, JGR, 123, 3919–3942.

Dong, C., Bougher, S. W., Ma, Y., et al. 2014, GRL, 41, 2708–2715.

Dubinin, E., Fraenz, M., Pätzold, M., et al. 2019, JGR, 124, 9725–9738.

Dubinin, E., Fraenz, M., Pätzold, M., et al. 2020, JGR, 125, e2020JA028010

Duru, F., Gurnett, D. A., Averkamp, T. F., et al. 2006, JGR, 111, A12204.

Duru, F., Gurnett, D., Morgan, D., et al. 2011, JGR, 116, A10316.

Egan, H., Jarvinen, R., Ma, Y., et al. 2019, MNRAS, 488(2), 2108–2120.

Ergun, R. E., Andersson, L. A., Fowler, C. M., et al. 2016, JGR, 121, 4668–4678.

Fallows, K., Withers, P., Morgan, D., et al. (2019). JGR, 124, 6029–6046.

Fan, K., Fraena, M., Wei, Y., et al. 2020, APJL, 898:L54 (7pp).

Fang, X., Ma, Y., Brain, D., et al. 2015, JGR, 120, 10,926 – 10,944.

Fang, X., Ma, Y., Masunaga, K., et al. 2017, JGR, 122, 4117 – 4137.

Gao, J. W., Rong, Z. J., Klinger, L., et al. 2021, Earth and Space Science, 8, e2021EA001860.

Gunell, H., Maggiolo, R., Nilsson, H., et al. 2018, Astron. Astrophys. 614, L3.

Gurnett, D. A., Kirchner, D. L., Huff, R. L., et al. 2005, Science, 310, 1929–1933.

Hess, S. L., Henry, R. M., & Tillman, J. E. 1979, JGR, 84(B6), 2923–2927.

Inui, S., Seki, K., Sakai, S., et al. 2019, JGR, 124, 5482–5497.

Langlais, B., Purucker, M. E., & Mandea, M. 2004, JGR, 109, E02008.

Li, S. B., Lu, H. Y., Cui, J., et al. 2020, EPP, 4(1), 1–9

Li, S. B., Lu, H. Y., Cao, J. B., et al. 2022, APJ, 931:30 (7pp)

Li, X. Z., Rong, Z. J., Gao, J. W., et al. 2020, EPP, 4(4), 1–9.

Li, Y., Lu, H. Y., Cao, J. B., et al. 2021, 921:139 (11pp).

Liu, D., Rong, Z. J., Gao, J. W., et al. 2021, APJ, 911:113 (10pp)

Ma, Y., Nagy, A. F., Sokolov, I. V., et al. 2004, JGR, 109, A07211

Ma, Y. J., Russell, C. T., Fang, X. H., et al. 2015, GRL, 42, 9113–9120.

Ma, Y., Dong, C., Toth, G., et al. 2019, JGR, 124, 9040-9057

Matta, M., Mendillo, M., Withers, P., et al. 2015, JGR, 120, 766–777

McFadden, J. P., Kortmann, O., Curtis, D., et al. 2015, *Space Science Reviews*, *195*(1-4), 199–256.

Mendillo, M., Lollo, A., Withers, P., et al. 2011, JGR, 116, A11303.

Nagy, A. F., Winterhalter, D., Sauer, K., et al. 2004, Space Science Reviews, 111, 33–114.

Najib, D., Nagy, A. F., Tóth, G., et al. 2011, JGR, 116, A05204

Ramstad, R., S. Barabash, Y. Futaana, H., et al. 2016, GRL, 43, doi:10.1002/2016GL070135

Ramstad, R., & Barabash, S. 2021, Space Science Reviews, 217(2), 1-39.

Sakai, S., Seki, K., Terada, N., et al. 2018, GRL, 45, 9336–9343.

Sakata, R., Seki, K., Sakai, S., et al. 2020, JGR. 125 (2), e2019JA026945.

Singh, R. N. and Prasad, R. J. 1983, Astrophys.4, 261–269

Schunk, R. W. and Nagy, A. F. (2009), Ionospheres, 2nd ed., Cambridge Univ. Press, New York

Weber, T., Brain, D., Xu, S., et al. 2020, GRL ,47, e2020GL087757

Withers, P., Flynn, C. L., Vogt, M. F., et al. 2019, JGR, 124, 3100–3109.

Weber, T., Brain, D., Xu, S., et al. 2021, JGR, 126, e2021JA029234

Wu, X. S., Cui, J., Xu, S. S., et al. 2019, JGR, 124, 734–751

Xu, S., Mitchell, D., Liemohn, M., et al. 2017, JGR, 122, 1831–1852

Xu, S., Mitchell, D. L., McFadden, J. P., et al. 2018, GRL, 45, 10,119–10,127.

Xu, S., Weber, T., Mitchell, D. L., et al. 2019, JGR, *124*, 1823 – 1842.

Appendix A:

This appendix depicts the magnetic field topology of the ESD around Mars (Figure A1) and the distributions of the total strength of magnetic field (including both the induced and the crustal magnetic field, Figure A2) and inclination angle (Figure A3) at 350 km, resulting from (a) observation and (b) simulations with the Gao's crustal magnetic field model and (c) the ESD model.

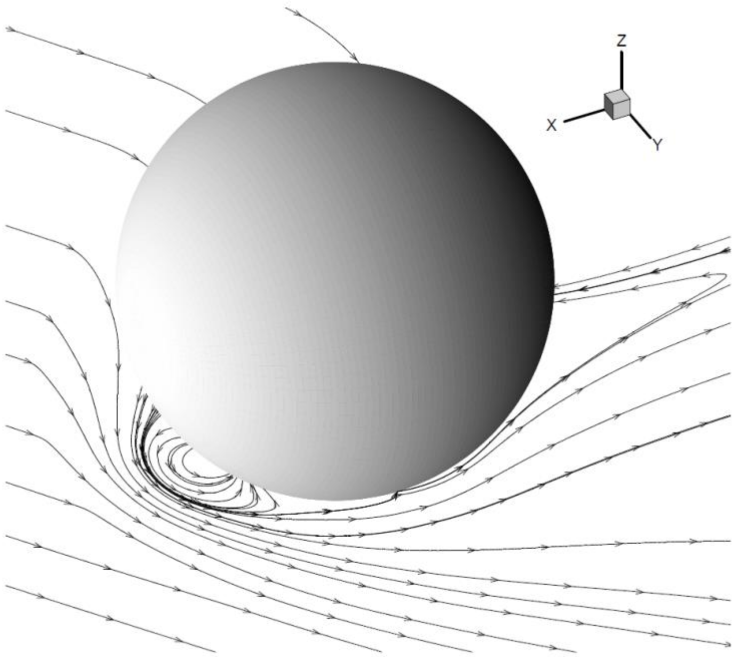

Figure A1. Magnetic field topology around Mars in the case with the ESD model.

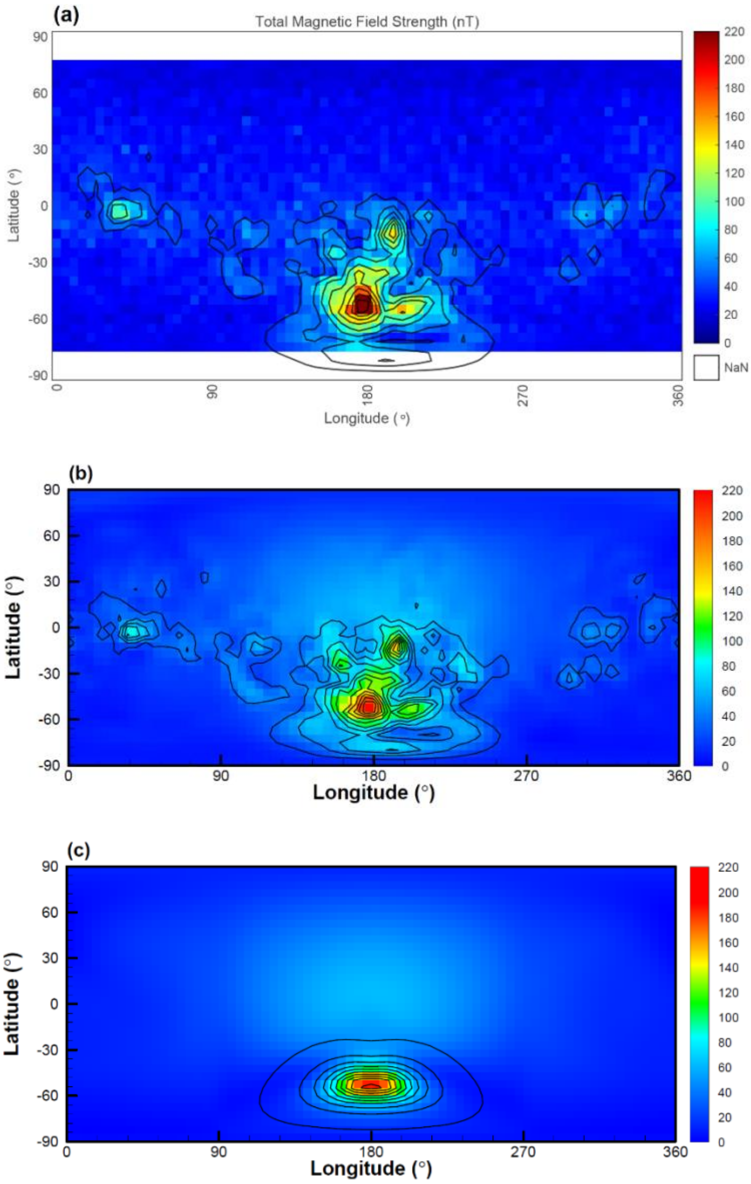

Figure A2. Total strength of magnetic field in the horizontal plane at 350 km, (a) based on the dayside MAVEN Magnetometer level 2 data and overlapped with isomagnetic lines of crustal field of Gao's model, (b) plotted from simulation with Gao's crustal field model and overlapped with its isomagnetic lines, (c) plotted from simulation with the ESD model and overlapped with its isomagnetic lines.

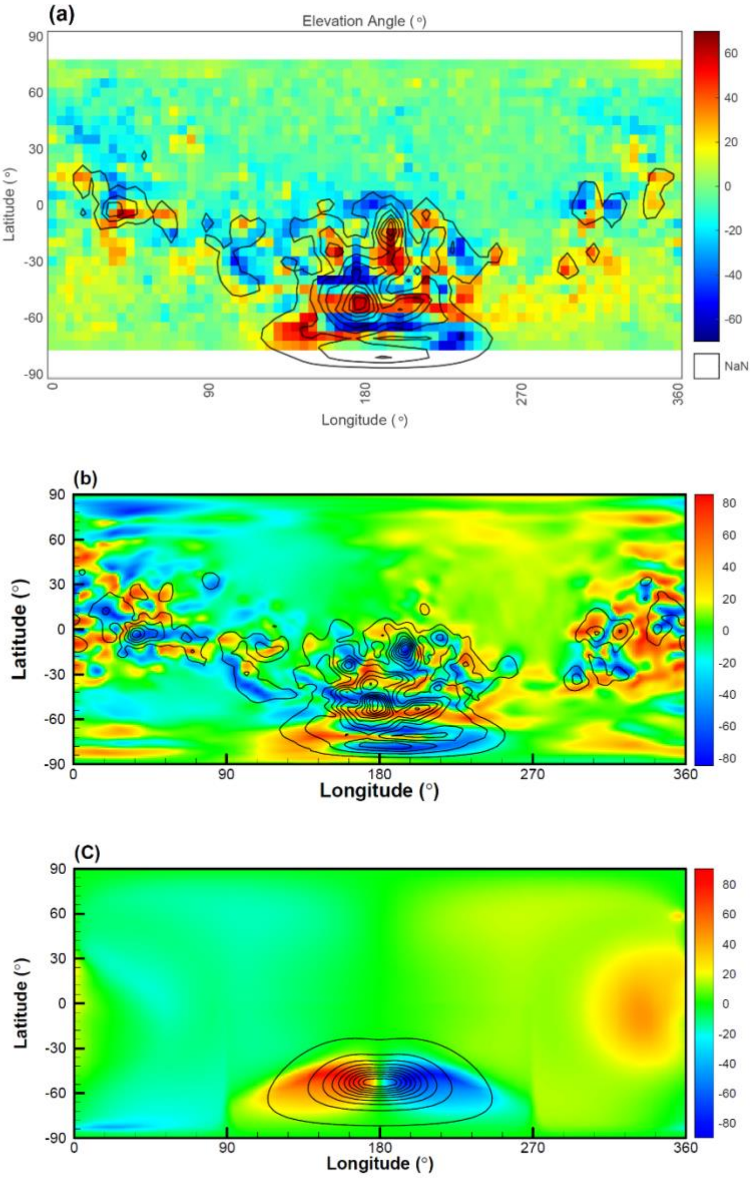

Figure A3. Magnetic elevation angle (also called inclination angle) in the horizontal plane at 350 km, (a) based on the dayside MAVEN Magnetometer level 2 data and overlapped with isomagnetic lines of crustal field of Gao's model, (b) plotted from simulation with Gao's crustal field model and overlapped with its isomagnetic lines, (c) plotted from simulation with the ESD model and overlapped with its isomagnetic lines.

Appendix B:

This appendix demonstrates the dayside O_2^+ velocity vector in the horizontal plane at 350 km derived from the multi-fluid MHD model without considering any Martian crustal field case.

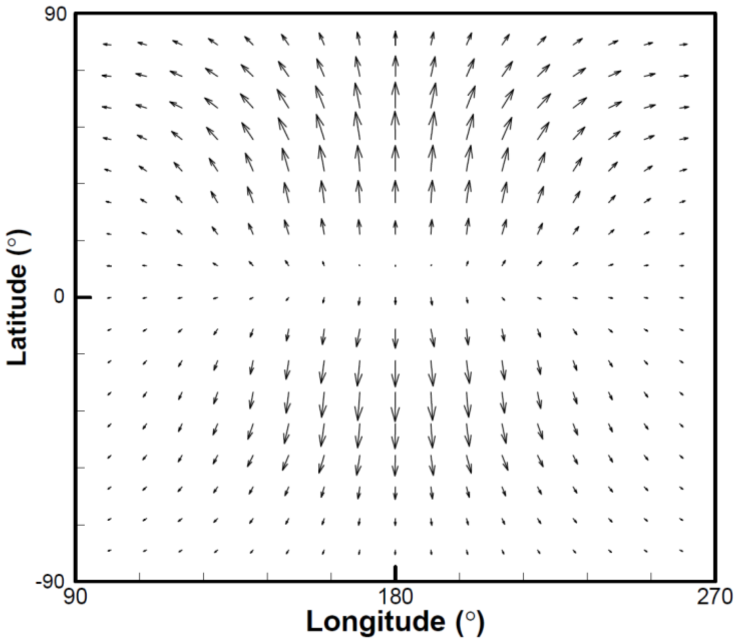

Figure B1. Dayside distribution of O_2^+ ion velocity vector (black anchor) at 350 km, resulting from simulation without crustal field model.